Environmental Earth Sciences (2018) 77:232
https://doi.org/10.1007/s12665-018-7325-6

ORIGINAL ARTICLE

Research on time–frequency analysis method of active earth pressure of rigid retaining wall subjected to earthquake

Yang Changwei[1] · Zhang Jianjing[1] · Wang Zhengzheng[2] · Cao Licong[1]

Received: 11 November 2015 / Accepted: 14 October 2016 / Published online: 16 March 2018

Abstract

Aiming at the drawback existing in the analysis methods of seismic active earth pressure of rigid retaining wall, the time–frequency computational method is proposed based on the elastic wave theory and Hilbert–Huang transform, which is full 3D nonlinear time history analysis method. It not only can consider the effect of three factors (peak ground acceleration, frequency and duration) of the bidirectional seismic wave on the seismic active earth pressure, but also can provide some valuable references for the time–frequency seismic design of other types of retaining structures. The reasonability of this method is verified by the shaking table test results, and it is more accurate than some representative methods such as limit equilibrium method and coordinated deformation method. At last, some rules and conclusions can be obtained by the parameters study, as shown in the following: With the increase in PGA, the critical rupture angle decreases, the resultant force of seismic active earth pressure increases, and its application point of resultant force gradually moves up; with the increase in frequency, the critical rupture angle and the resultant force of seismic active earth pressure are distributed in the shape of saddle and the handstand saddle, respectively. And they achieve the maximum value when the frequency is close to natural frequency of rigid retaining wall, but the application point essentially is unchanged.

Keywords Rigid retaining wall · Seismic active earth pressure · Hilbert–Huang transform · Time–frequency analysis method

Introduction

Earthquake-induced landslides (Keefer 1984; Hutchinson 1987; Sassa 1996; Rodriguez et al. 1999; Prestininzi and Romeo 2000; Chigira et al. 2010) can result in great damages and losses (Bird and Bommer 2004). They have been documented for some historical earthquakes such as the 2008 "Wenchuan" earthquake in China (Zhang et al. 2007), Chi-Chi earthquake in Taiwan (Khazai and Sitar 2003) and Northridge earthquake in America (Jibson et al. 2000). On May 12, 2008, the Ms 7.9 (Magnitude 7.9 2008) Wenchuan earthquake occurred in the Longmenshan region at the eastern margin of the Tibetan Plateau, adjacent to the Sichuan Basin (see Fig. 1). It triggered a large number of earth retaining walls damage, landslides, debris flows, etc., which directly led to 69,200 fatalities, 18,195 persons missing, 374,216 persons injured, 5,362,500 collapsed homes and 21,426,600 homes that badly damaged, and more than five million people left homeless (Cui et al. 2009).

After every large earthquake, the field investigation should be carried out as early as possible. On May 14, 2008, a careful field investigation was settled on along the national, provincial roads and part of the county road about 2661 km long, see in Figs. 2, 3 and 4. The investigated results show that the rigid retaining including gravity retaining wall and gravity balanced retaining wall suffered the most severe damage during the earthquake. And it suffered the most serious seismic damage. The total of investigated retaining wall is 343, and

✉ Wang Zhengzheng
txh19950818@163.com

Yang Changwei
yangchangwei56@163.com

Zhang Jianjing
1209732335@qq.com

Cao Licong
827169243@qq.com

[1] School of Civil Engineering, Key of Transportation Tunnel Engineering, Ministry of Education, Southwest Jiaotong University, Chengdu 610031, China

[2] School of Civil Engineering, Dalian University of Technology, Dalian 116024, China

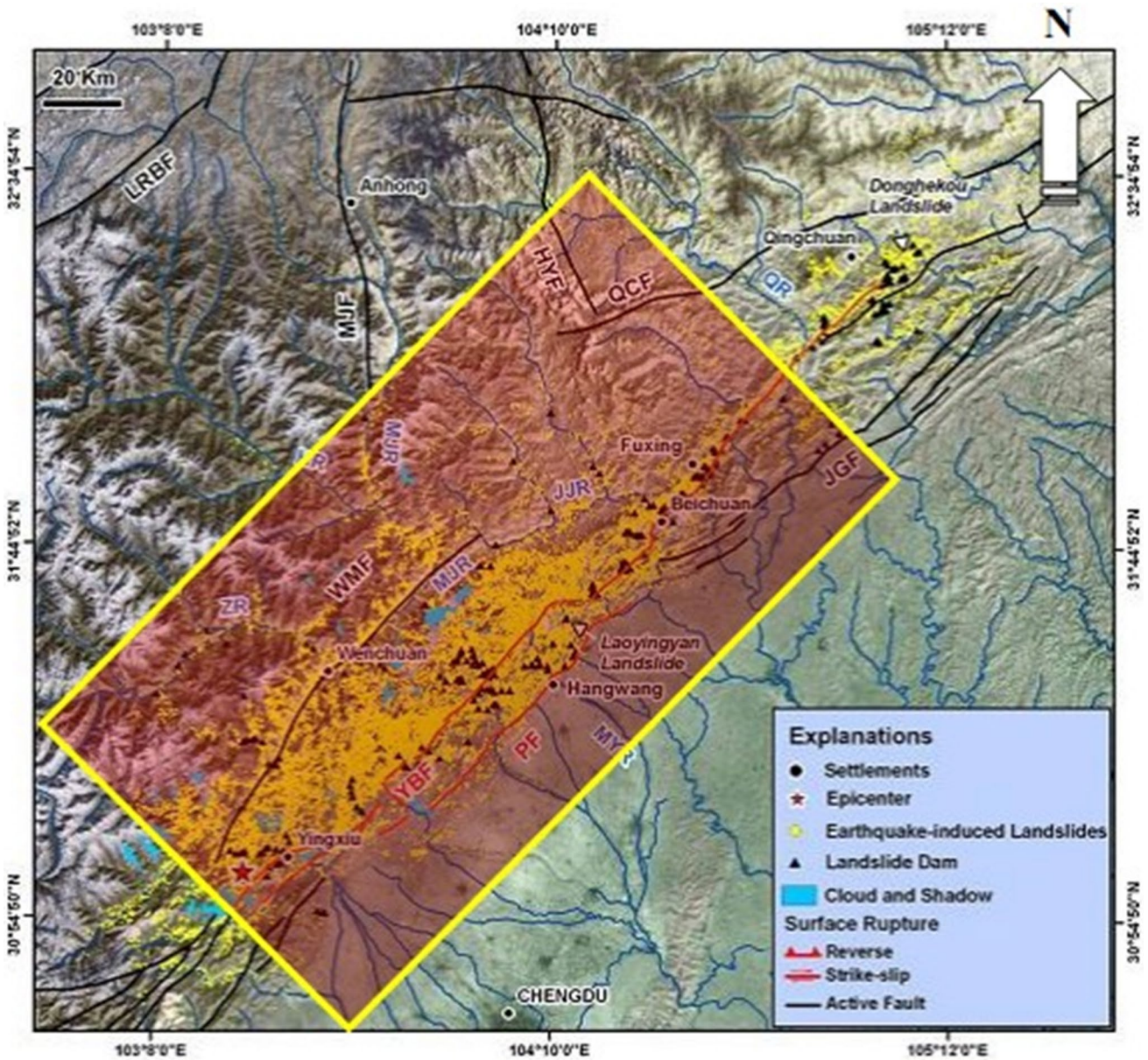

Fig. 1 Field investigation area and 12 May 2008 Wenchuan earthquake fault surface rupture map

98.6 percent of that have been damaged. While the flexible retaining wall such as reinforced soil retaining wall and pile slab retaining wall only had a total of only 4 damage. The above-mentioned phenomenon is mainly caused by site conditions, seismic capacity and earthquake (Güllü et al. 2008; Güllü and Pala 2014; Güllü 2012, 2013, 2014a, b, 2015; Güllü and Girisken 2013; Güllü and Khudir 2015; Güllü and Iyisan 2016; Cui et al. 2017; Gou et al. 2017, 2018).

However, site conditions together with their seismic capacity are more important than earthquake, because we have to always live under earthquake (Ansal et al. 2001; Hazirbaba and Gullu 2010; Gullu and Hazirbaba 2010; Güllü and Erçelebi 2007). Thus, we have to design good retaining structures in order to reduce the losses of life and property. And then, the reasonable design method of retaining structures is very important. So far, most researchers mainly concentrate their attention on three fields: The first one is limit equilibrium method (Choudhury and Nimbalkar 2006; Kumar 2001; Madhav and Kameswara 1969), which assumes the relative movement between the wall and the earth filling is sufficiently large. And the stress–strain of soil will reach the limit or damage state. The representative research result is Mononobe–Okabe seismic earth pressure theory (Mononobe 1924; Okabe 1924). The second one is coordinated deformation method, considering the wall–soil interaction and the actual stress–strain properties of soil

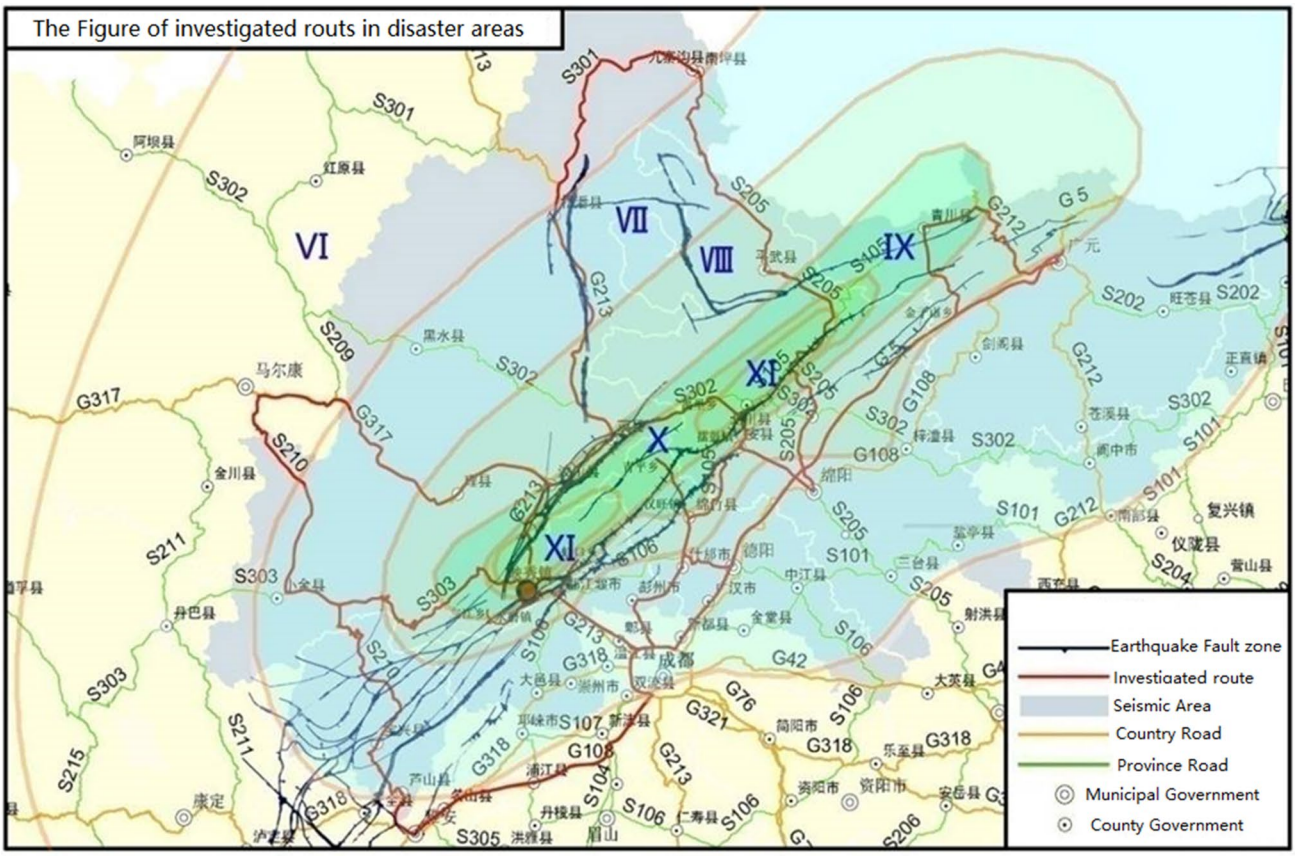

Fig. 2 Roads investigated and seismic intensity

Fig. 3 Field investigations in hazard point no. 30

Fig. 4 Earthquake damage cases

(Newmark 1965; Choudhury and Singh 2006; Siddharthan and Norris 1992; Zeng and Steedman 2000). The third one is finite element method (Smith and Wu 1997; Richards and Elms 1979), such as finite element method established by Clough and Duncan (Clough and Chopra 1966), which considered the actual stress–strain relationship of soil.

Among these methods, the limit equilibrium method can only take into account the effect of peak ground acceleration (PGA) on the seismic earth pressure of retaining wall, but cannot take into account the influence of seismic wave frequency and duration time on the earth pressure of retaining wall. The coordinate deformation method cannot consider

the influence of duration and frequency of seismic wave for earth pressure acting on retaining wall and has inconvenience and low calculation accuracy in actual engineering. Although the finite element method is able to consider the amplitude, frequency and duration of the seismic wave, the operation process is very complicated, especially for the wall and soil contact surface.

At the same time, the analysis results of failure mechanism reveal the main damages were caused by elastic wave–SV wave. However, the SV wave is a complex non-stationary signal, and its frequency characteristics change with time and cause the limitation of the equilibrium method and the coordinated deformation method. Therefore, the time-frequency computational method of seismic active earth pressure of rigid retaining wall subjected to SV wave will be proposed based on the elastic wave prorogation theory (Du 2009) and Hilbert–Huang transform (HHT, Huang et al. 1998).

Time–frequency computational method of seismic active earth pressure of rigid retaining wall

Basic assumption

The derivation of this method is based on the following hypotheses: (1) The field investigation results about retaining wall during 12 May 2008 Wenchuan earthquake show that the main damage forms of gravity retaining wall and gravity-balanced retaining wall are rigid body motions such as slippage, rotation, overturn and cracking. They usually occur brittle rupture, and there is only a tiny deformation. At the same time, almost all of the computational methods of seismic active earth pressure of retaining wall assume the earth retaining wall is rigid (Choudhury and Nimbalkar 2006; Kumar 2001; Madhav and Kameswara 1969; Mononobe 1924; Okabe 1924). Therefore, the earth retaining wall is rigid; (2) the backfill soil is single, homogeneous and isotropic; and (3) when the wall move forward or backward, the sliding soil wedge behind the wall will slide along the plane from the wall back to the wall heel. (4) Seismic action will not affect the basic mechanical properties of soil; (5) the material damping of the soil behind the wall will cause a large consumption of the seismic wave energy, which makes the reflection seismic wave on the surface of the earth to carry a very weak seismic energy and to prorogate downward (Yang et al. 2015, 2016, 2018). Therefore, the formula derivation in this paper does not consider the influence of the element soil caused by the reflection wave from the surface of the backfill.

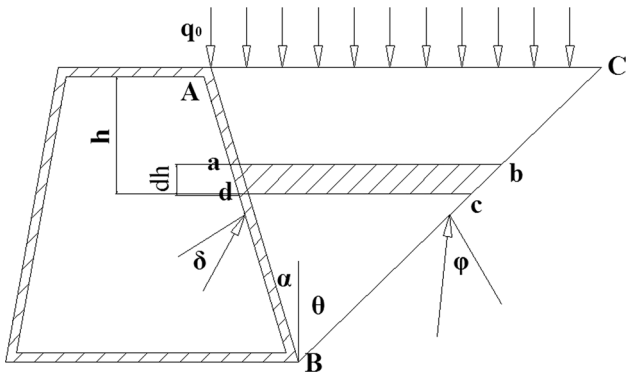

Fig. 5 Stress analysis model of rigid retaining wall

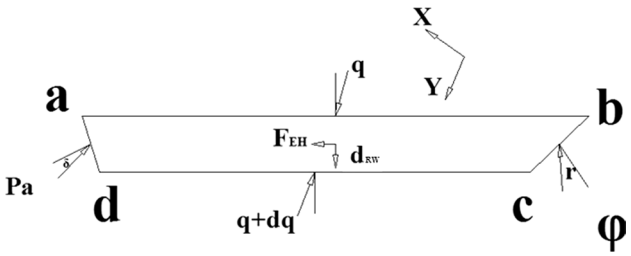

Fig. 6 Stress analysis model of horizontal element

Generalized analysis model

The applicability of generalized analysis model contains the gravity earth retaining wall, gravity-balanced retaining wall, overhanging wall and cantilever retaining wall, etc. The calculation model of the active earth pressure is shown in Fig. 5. The horizontal slice method is used for the horizontal layering element and it is selected to research, as seen Fig. 6. The parameters in Figs. 5 and 6 are shown as follows: α is the dip angle of retaining wall back, φ is the inner friction angle, δ is outer friction angle, q_0 is uniform surcharge, P_a is active earth pressure strength, d_{Rw} is the weight of soil slices d_w minus the vertical inertia force acting on the soil F_{EV}, dh is the thickness of soil slices, q and $q + dq$ are the resultant forces of the two sides of the soil slices, respectively; r is the resultant force of normal force and tangential force of sliding surface; and F_{EH} is the horizontal inertia force acting on the soil. The stress analysis of the horizontal soil slices induced by the force of dynamic wave is shown in Fig. 7. It is worth noting that the inertia force in the element was replaced by undulation force in seismic waves. In addition, since the focus of this paper is the response to the ground motion of rigid retaining wall under the action of SV wave, the basic characteristic of SV wave is that the direction of propagation is perpendicular to the direction of movement. Therefore, the direction of movement of element level is

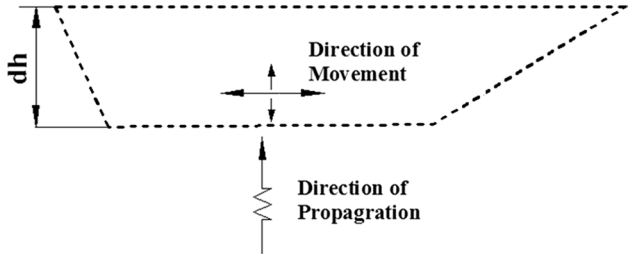

Fig. 7 Analysis model of the horizontal soil bar under the undulation force

horizontal and the seismic wave propagation direction is vertical, as shown in Fig. 5.

Seismic earth pressure of retaining wall

As shown in Fig. 5, the geometric relationships among the various dimensions of the model can be obtained. And then, select the horizontal soil element *abcd* as research object and establish the static equilibrium equations. At last, combined with the boundary conditions, when $h = 0$, $q = q_0/\cos\eta$, the seismic active pressure strength can be obtained as follows:

$$\left.\begin{aligned} P_{\mathrm{a}} &= m_{a1}(H-h)^{-A1} - m_{a2}(H-h) \\ m_{a1} &= na_1\left(\gamma_R \frac{1}{\cos\eta}\frac{H}{1+A_1} + \frac{q_0}{\cos\eta}\right)\cdot H^{A_1} \\ m_{a2} &= na_1\gamma_R \frac{1}{\cos\eta}\frac{1}{1+A_1} \\ \gamma_R &= \gamma - \omega^2 V(z) \\ A_1 &= 1 - \frac{\cos(\theta+\varphi-\eta)}{\cos\theta}\cdot\frac{\cos\theta\sin(\alpha+\eta)-\cos\alpha\sin(\theta-\eta)}{\sin(\alpha+\delta)\cos(\theta+\varphi-\eta)-\sin(\theta+\varphi)\cos(\alpha+\delta+\eta)} \\ &\quad\cdot\frac{\cos\theta\sin(\alpha+\theta+\varphi+\delta)}{\cos(\theta+\varphi-\eta)\sin(\alpha+\theta)} \end{aligned}\right\} \quad (1)$$

Note any acceleration at any time during the ground motion process can be decomposed into superposition of several simple harmonic motions, and arbitrary harmonic motion displacement potential function can be written as:

$$u(z,t) = U(z)e^{i\omega t}, \quad (2)$$

where $u(z, t)$ is the horizontal displacement function of the element, $U(z)$ is the horizontal elastic displacement amplitude of element, and ω is the horizontal vibration frequency of the element. In this paper, the horizontal displacement potential function of SV wave is expressed by the horizontal elastic displacement and has several frequencies at any moment, which change gradually with time. The results of the method mentioned above basically agree with the results in the literature (Ma and Wu 2000; Liao 1996). So the horizontal inertia force induced by SV wave in the element soil is:

$$F_{EH} = \left| dw \cdot \frac{\partial^2 u}{\partial t^2}/g \right| = dw \cdot \omega^2 U(z)/g. \quad (3)$$

And then, the vertical inertia force induced by SV wave in the element soil is:

$$F_{EV} = \left| dw \cdot \frac{\partial^2 v}{\partial t^2}/g \right| = dw \cdot \omega^2 V(z)/g, \quad (4)$$

where $V(z)$ is the vertical elastic displacement amplitude of element and ω is the vertical vibration frequency of the element. Therefore, the seismic angle η is as follows:

$$\tan\eta = F_{EH}/d_{Rw} = \frac{dw\cdot\omega^2 U(z)}{g}/(dw - dw\cdot\omega^2 V(z)/g). \quad (5)$$

Resultant force of seismic active earth pressure and its action point

The resultant force of active earth pressure:

$$E_a = \int_o^H \frac{P_a}{\cos\alpha}\mathrm{d}h = \frac{1}{\cos\alpha}\left[\frac{m_{a1}H^{1-A_1}}{1-A_1} - \frac{1}{2}m_{a2}H^2\right]. \quad (6)$$

The distance from the position of resultant force of active earth pressure to the wall heel is:

$$Z_{0a} = \frac{\int_0^H \frac{P_a(H-h)}{\cos\alpha}\mathrm{d}h}{\int_0^H \frac{P_a}{\cos\alpha}\mathrm{d}h} = \frac{\frac{m_{a1}H^{-A_1}}{2-A_1} - \frac{m_{a2}H}{3}}{\frac{m_{a1}H^{-A_1}}{1-A_1} - \frac{m_{a2}H}{2}}H. \quad (7)$$

In summary, substituting the parameters n_{a1}, n_{a2}, m_{a1}, $A1$, $q1$ into Formula (6) it can be written as follows after simplification.

$$E_a = \frac{\gamma_R H^2}{2\cos\eta}\frac{\sin(\alpha+\theta)\cos(\theta+\varphi-\eta)}{\cos\alpha\cos\theta\sin(\alpha+\theta+\varphi+\delta)} + \frac{q_0 H}{\cos\eta}\frac{\sin(\alpha+\theta)\cos(\theta+\varphi-\eta)}{\cos\eta\cos\alpha\cos\theta\sin(\alpha+\theta+\varphi+\delta)}, \quad (8)$$

in which $\eta = \arctan(F_{EH}/d_{Rw}) = \arctan\left[\frac{dw\cdot\omega^2 U(z)}{g}/(dw - dw\cdot\omega^2 V(z)/g\right]$.

Critical rupture angle

According to the basic principle of active earth pressure (Lu 2002), among all the possible rupture angles θ, there is an angle θ which leads to the maximum earth pressure. From Formula (8) we can know that if $\mathrm{d}E_a/\mathrm{d}\theta$ is equal to zero, the critical rupture angle which can lead to the maximum earth pressure can be calculated. However, it is hard to get explicit solution. Therefore, based on the graphical method from the literature (Lin et al. 2010), the explicit solution for critical rupture angle of seismic active earth pressure is shown in Formula (9) as follows:

$$\tan\theta_{acr}=\frac{\sqrt{\frac{\sin(\alpha+\delta)\cos(\alpha+\delta+\eta)}{\cos\alpha\sin(\varphi-\eta)}}-\cos(\alpha+\delta)\sin(\alpha+\varphi+\delta)}{\cos(\alpha+\delta)\cos(\alpha+\varphi+\delta)}. \tag{9}$$

Note the applicability of time–frequency computational method of seismic active earth pressure of rigid retaining wall is shown in the following. The critical rupture angle of seismic active earth pressure must satisfy the following conditions: $\alpha+\delta+\eta\le 90°$ and $\varphi\ge\eta$.

Time–frequency effect of seismic wave

Based on the above derivation process, the time–frequency effect of seismic wave is directly reflected in the elastic displacement amplitude $U(z)$ and the frequency of the input seismic wave, and indirectly reflected in the solution of the seismic angle in the seismic active earth pressure formula. Therefore, the solving flow is put forward, as follows. Firstly, the seismic wave is decomposed into several intrinsic mode functions (IMF) by empirical mode decomposition (EMD); secondly, multichannel signal composed by several single-channel signals is converted into a single-channel signal composed by single IMF; thirdly, solve the instantaneous frequency of each channel and draw the time–frequency curve of each IMF; fourthly, substitute every IMF and its instantaneous frequency into Formulas (2)–(4) to get every solution and then add all the solutions together to obtain the seismic angle of rigid retaining wall under seismic action. Finally, substitute relevant parameters into formula of (9), (1), (8) and (7) to calculate the critical rupture angle of active earth pressure, the resultant force and its position of the active earth pressure, respectively.

In summary, the time–frequency calculation method for seismic active earth pressure of rigid retaining wall is able to compensate the limitations that exist in the equilibrium method and coordinated deformation method, which had a good consideration of the influence of PGA, frequency and duration on the seismic active earth pressure of rigid retaining wall. In the following, Wolong–Wenchuan earthquake wave is taken as an example to illustrate and detail, as shown in the following: Firstly, input the Wolong–Wenchuan earthquake wave, as shown in Figs. 8, 9 and 10; secondly, decompose the seismic wave by EEMD and obtain the IMF, as shown in Fig. 11; and finally, calculate the instantaneous frequency of each IMF, as shown in Fig. 12.

Solving flow

In summary, the solving flow of time–frequency calculation method of active earth pressure of rigid retaining wall is shown in Fig. 13.

Verification of time–frequency calculation method by shaking table test results

Because of the strong randomness of earthquake, doing the site test is scarcely possible. Therefore, in order to verify the accuracy of time–frequency method of seismic active earth pressure for rigid retaining wall, this paper carried out a large shaking table test based on the similar system. The prototype of the test is a 9.6-m-high rigid retaining wall located in G213. The geometric similarity ratio on the test is 1:6. The seismic wave used in the test is the compression wave of the horizontal Wolong–Wenchuan earthquake wave, horizontal Kobe earthquake wave and horizontal El Centro earthquake wave with the time similarity 1:2.45, as shown in Figs. 14, 15, 16, 17, 18 and 19. The similar material mainly consists of quartz sand, barite powder and water according to a certain proportion. The similarity ratio of unit weight, internal friction angle and Poisson for the similar material

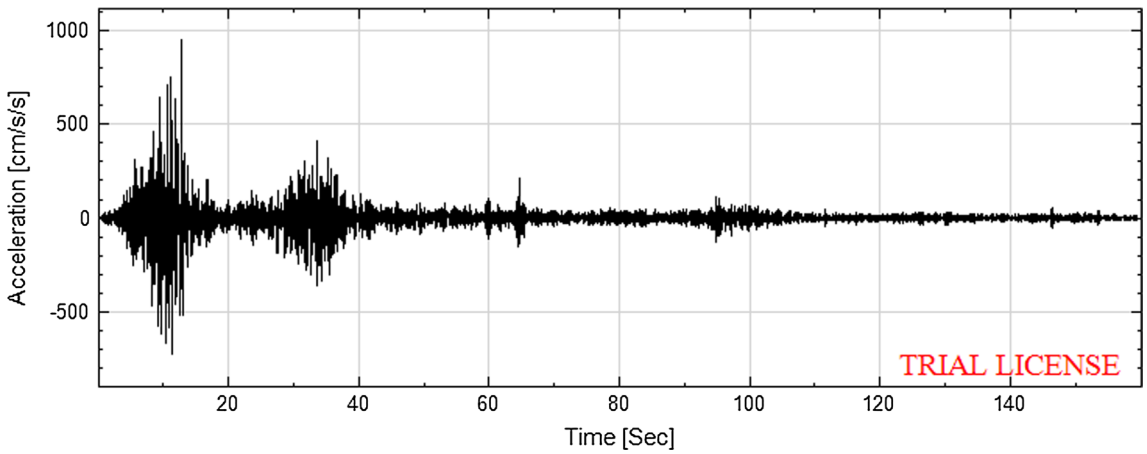

Fig. 8 Horizontal acceleration–time history of Wenchuan–Wolong earthquake

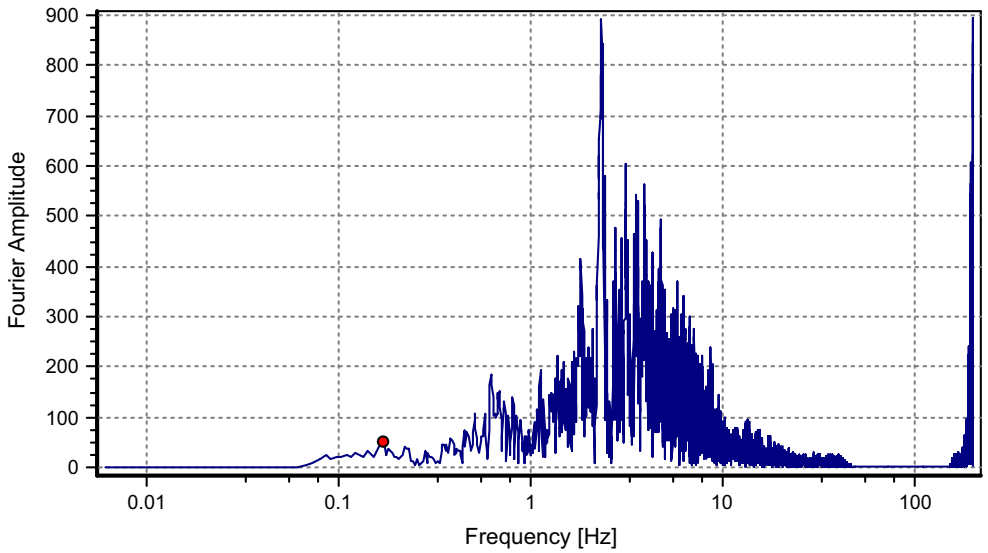

Fig. 9 Fourier spectrum of horizontal Wenchuan–Wolong earthquake wave

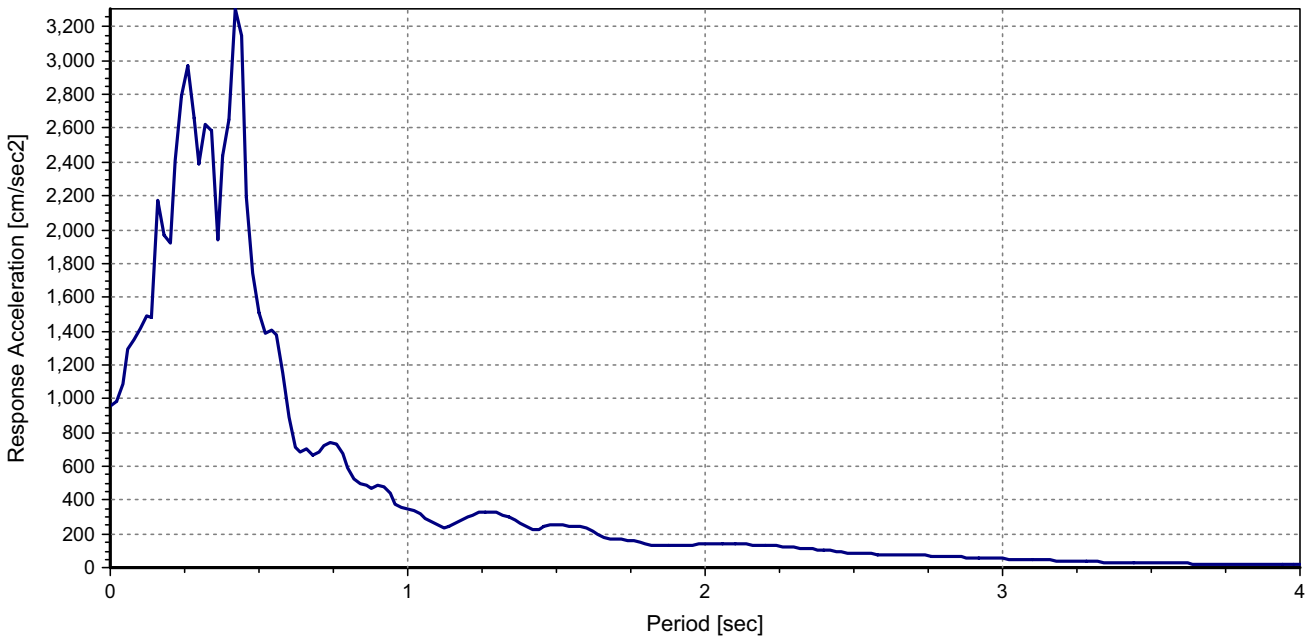

Fig. 10 Spectrum of horizontal Wenchuan–Wolong earthquake wave

are 1:1. The rigid model box used in shaking table test is made of steel plate, steel and organic glass with the inner size of 1.5 m × 3.7 m × 2.1 m (length × width × height). In order to reduce the reflection of the vibration wave at the boundary, a 30-mm-thick polystyrene foam cushion is place behind the soil to simulate absorbing material. At the same time, based on the similar ratio, the size of the retaining wall model is 1.6 m (high) × 1.5 m (wide), the top width of the wall is 0.33 m, the bottom width of the wall is 0.55 m, the height of the wall at the toe is 0.204 m, and the width of the wall at the toe is 0.102 m. The retaining wall model is made of fine-grained concrete, and the filling material is made of dry sand. The filling material of the subgrade model in the model box should be compacted after layering, which can ensure that the degree of compaction of the foundation soil and the backfill soil behind the wall is consistent with the actual engineering condition. In order to monitor the earth pressure of retaining wall more accurately, 2 rows of sensors are arranged on the back of the wall. Each row is arranged with 6 sensors: One row is arranged with strain-type soil

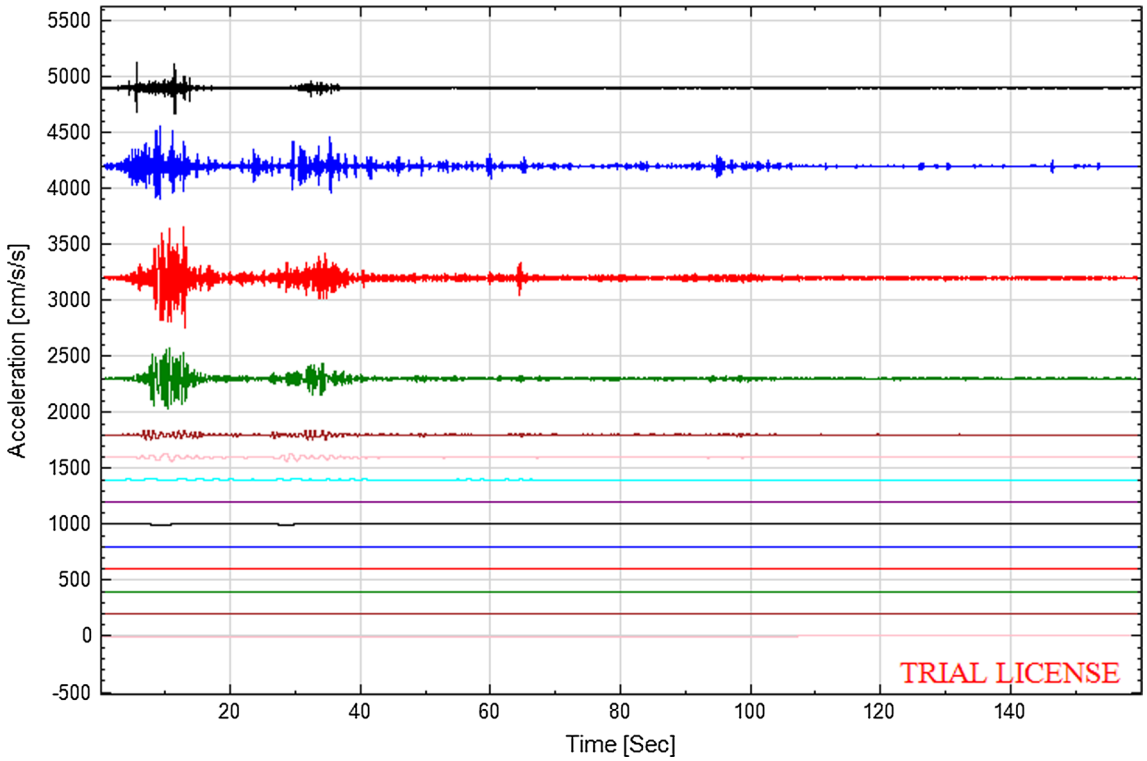

Fig. 11 Horizontal acceleration–time history of IMF

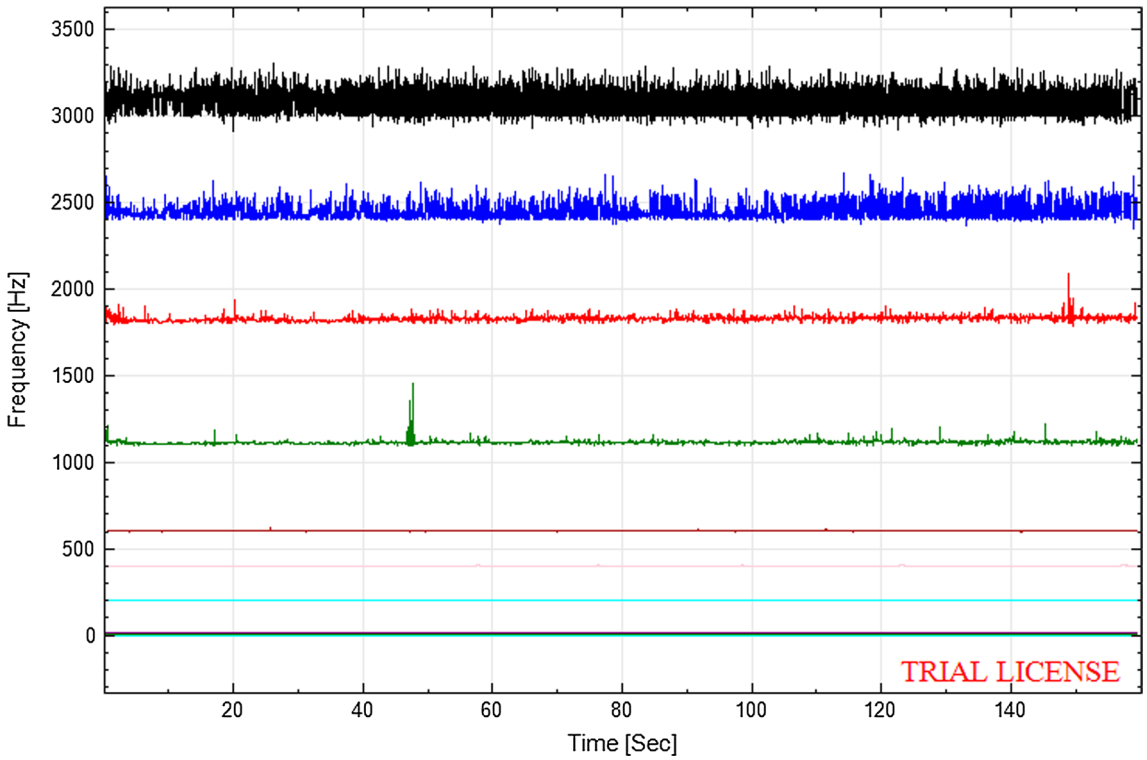

Fig. 12 Frequency–time history of IMF

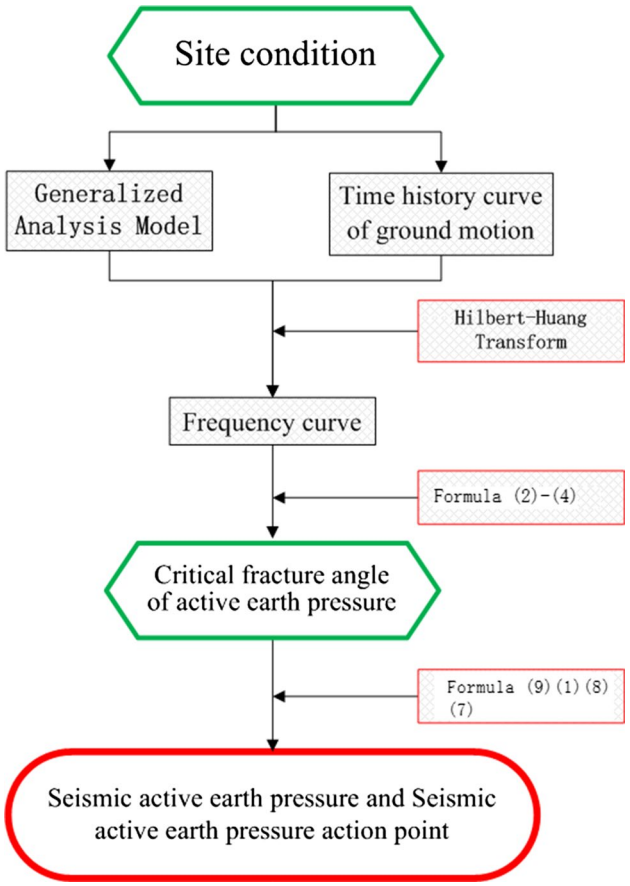

Fig. 13 Flowchart of time–frequency analysis method of active earth pressure of rigid retaining wall subjected to earthquake

pressure sensor and the other row is arranged with piezoelectric-type earth pressure sensor. The specific physical and mechanical parameters are shown in Table 1, the vibration table test model is shown in Fig. 20, and the sensor placement is shown in Fig. 21.

Based on the time–frequency calculation method proposed in this paper, the correlation parameters were substituted into Formulas (6) and (7) to calculate the resultant force of seismic active earth pressure and its action point under different PGA (0.1, 0.2, 0.4 and 0.7 g) of Wolong–Wenchuan earthquake waves, Kobe earthquake wave and El Centro earthquake wave. At the same time, in order to reflect the advantage of time–frequency analysis method, some representative methods are used to calculate the seismic active pressure and its action point, such as limit equilibrium method (Choudhury and Nimbalkar 2006) and coordinated deformation method (Siddharthan and Norris 1992). The specific calculation results and the shaking table test result are shown in Tables 2, 3 and 4, respectively.

The analysis results are given in Tables 2, 3 and 4: While Wolong–Wenchuan earthquake wave is input, for the time–frequency analysis method, the maximum error of the resultant force of active earth pressure and its acting position of the rigid retaining wall is 8.36 and − 8.82%, respectively; the minimum error can reach 5.84 and 2.94%, respectively. For the limit equilibrium method, the maximum error of the resultant force of active earth pressure and its acting position of the rigid retaining wall is − 32.55 and − 32.35%, respectively; the minimum error can reach − 6.93 and − 13.16%, respectively. For the coordinated deformation method, the maximum error of the resultant force of active earth pressure and its acting position of the rigid retaining wall is 12.04 and − 23.53%, respectively; the minimum error can reach 5.93 and 7.69%, respectively. For the time–frequency analysis method, the maximum error is smaller than 10%, so this method is correct and the calculation results are credible. At the same time, the time–frequency analysis method is more accurate than the limit equilibrium method and coordinated deformation method, which can also be obtained from the results when the input wave is Kobe earthquake wave and El Centro earthquake wave. Besides, when the input wave is changed, the results are constant when using the limit

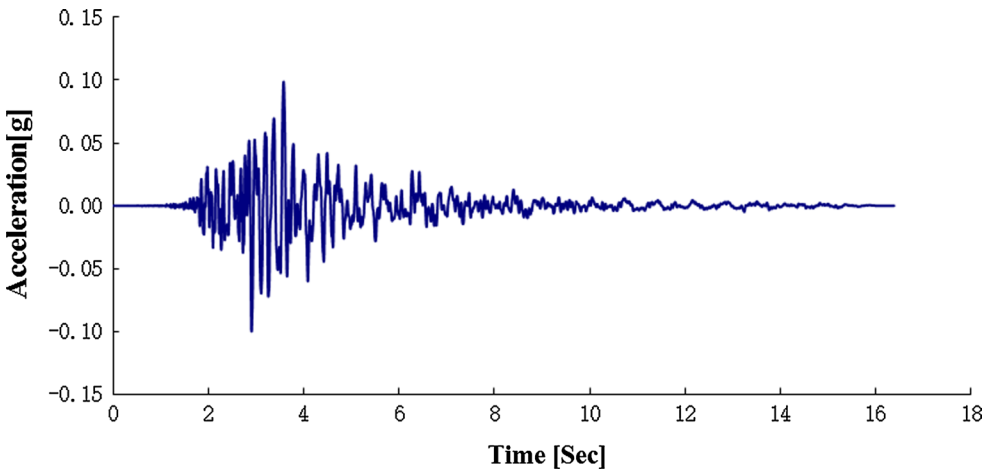

Fig. 14 Horizontal acceleration–time history of Wenchuan–Wolong earthquake wave (0.1 g)

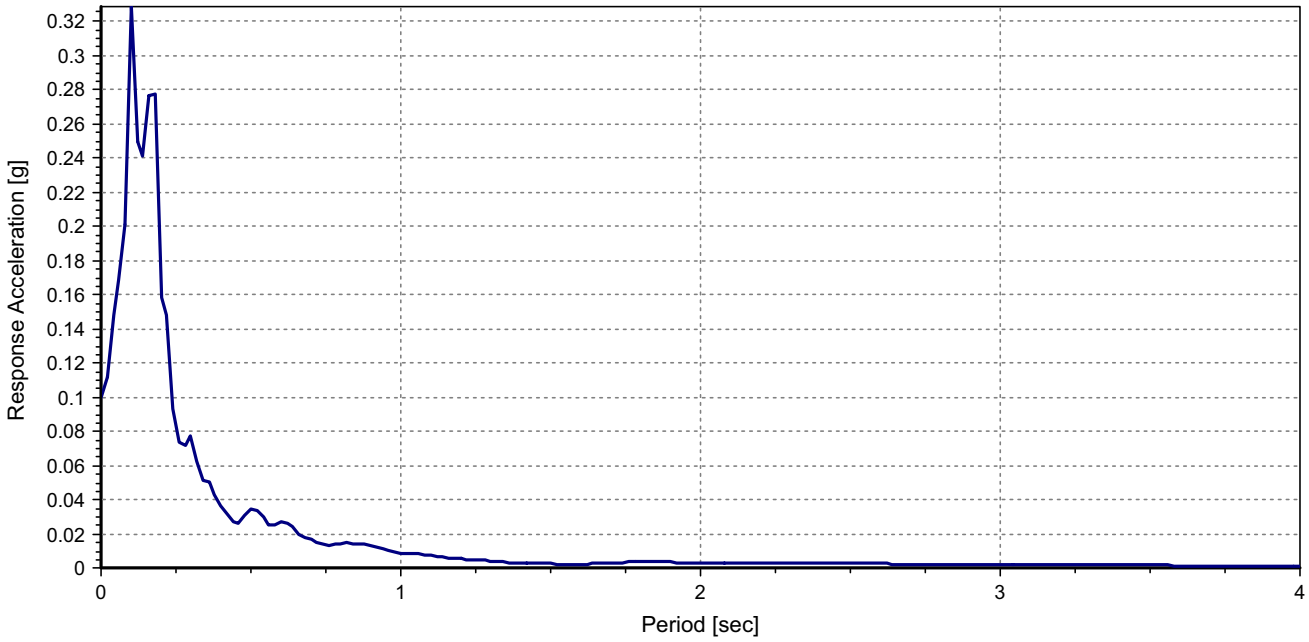

Fig. 15 Response spectra of horizontal Wenchuan–Wolong earthquake wave (0.1 g)

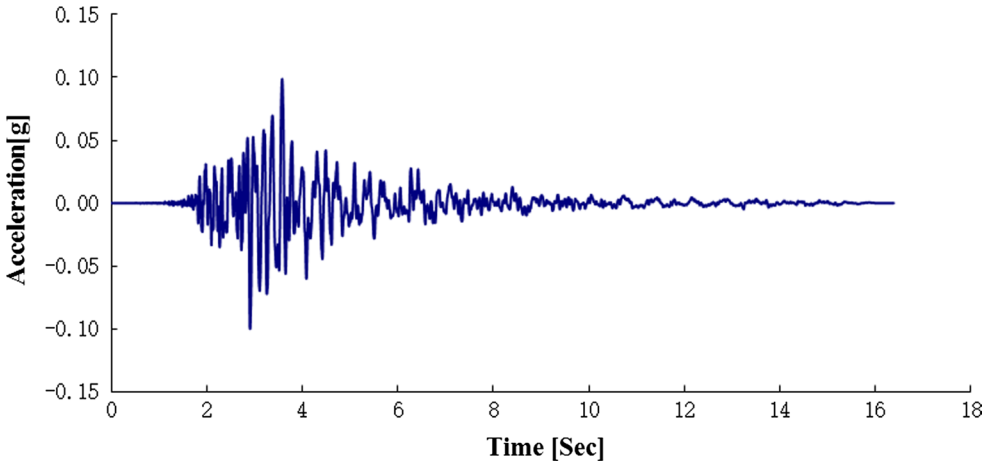

Fig. 16 Horizontal acceleration–time history of Kobe earthquake wave (0.1 g)

equilibrium method and coordinated deformation method to calculate, but the results of time–frequency method change with the seismic wave type. This fully shows the time–frequency can consider the effect of frequency and duration on seismic active earth pressure, which is an important advantage of time–frequency analysis method.

Parameter discussion

For the time–frequency calculation method of seismic active earth pressure of rigid retaining wall, the influence of different loading frequencies on the critical rupture angle, active earth pressure, active earth pressure and the action point of seismic active earth pressure is analyzed in this paper. The concrete calculation examples are shown as follows: The rigid retaining wall height H is 5 m, the unit backfill soil γ is 17 kN/m^3, cohesive force c is 0, the internal friction angle φ is 33°, the wall back is vertical, the filling surface is horizontal with no overload, the peak ground motions are 0.1 and 0.2 g and 0.4 g horizontal sine wave without vertical sine wave, and the frequency of sine wave is 0.1, 0.2, 0.4 Hz and 0.8, 1.0, 2, 4 and 5 Hz and 6, 8, 10 Hz. The concrete calculation results are shown in Figs. 22, 23, 24, 25.

The conclusions drawn from Figs. 22, 23, 24 and 25 are shown as follows: (1) With the increase in seismic intensity, the resultant force of active earth pressure gradually increases. Meanwhile, the critical rupture angle gradually

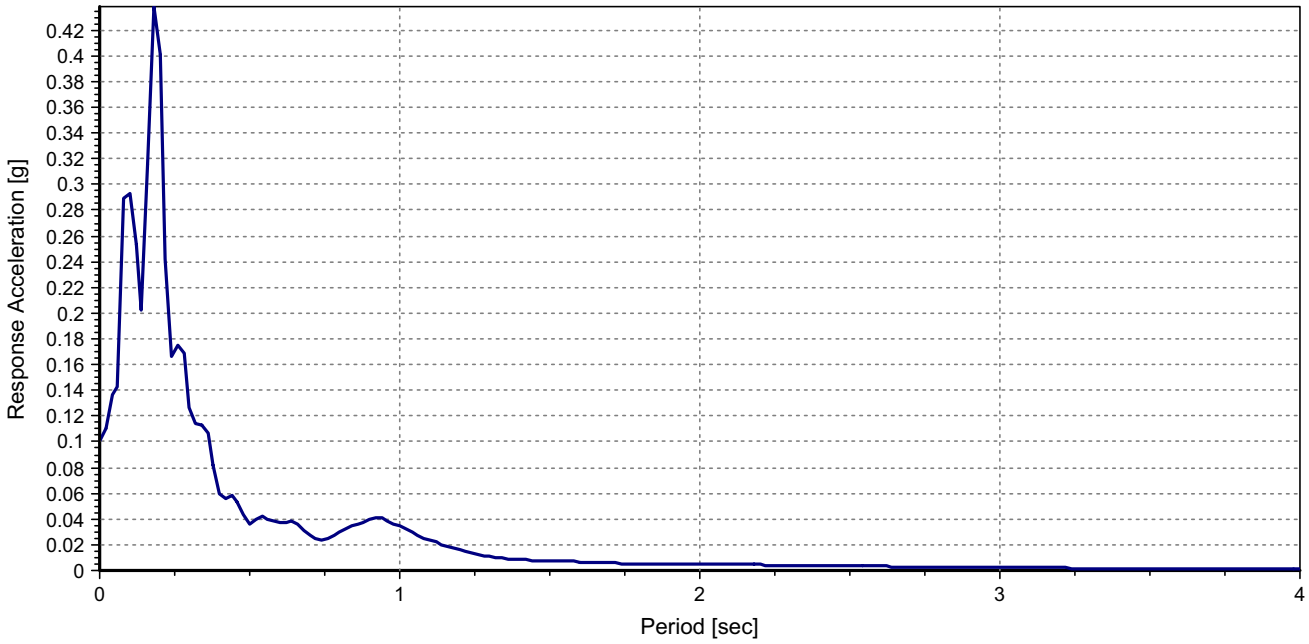

Fig. 17 Response spectra of horizontal Kobe earthquake wave (0.1 g)

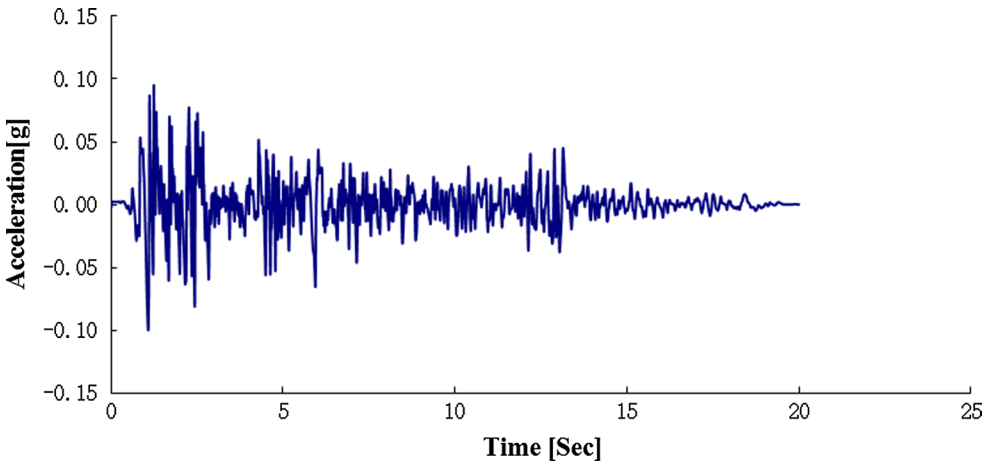

Fig. 18 Horizontal acceleration–time history of El Centro earthquake wave (0.1 g)

decreases and the action position of resultant force gradually shifts up. (2) With the increase in frequency, the critical rupture angle and seismic active earth force was "inverted saddle shape" and "positive saddle shape" distribution, reaching the maximum when $f = 1$ Hz. The phenomenon may be interpreted with resonance. When the input of seismic wave frequency $f = 1$ Hz, the resonance may happen because the self-vibration frequency f of rigid retaining wall system is equal to 1.32 Hz, which intensifies the seismic response of rigid retaining wall system and causes the critical rupture angle decreases and the earth pressure force increases. (3) With the increase in frequency, the action position of resultant force is basically unchanged, and the fluctuation is small. The reason for this phenomenon is shown as follows: The frequency of seismic wave has a significant influence on the size of earth pressure, while the influence on its distribution is small. Therefore, the action position basically is not changed with the input frequency. (4) In the case of rigid retaining wall, the ratio of resultant force obtained by the method proposed in the paper to that obtained by the design code under different seismic intensities and different frequency ranges from 1.0 to 1.3 and the position of resultant force is basically the same. The results fully illustrate that the seismic stability design of rigid retaining wall only considers peak ground motion and ignores the frequency, and may reduce the seismic safety reservation of the retaining wall.

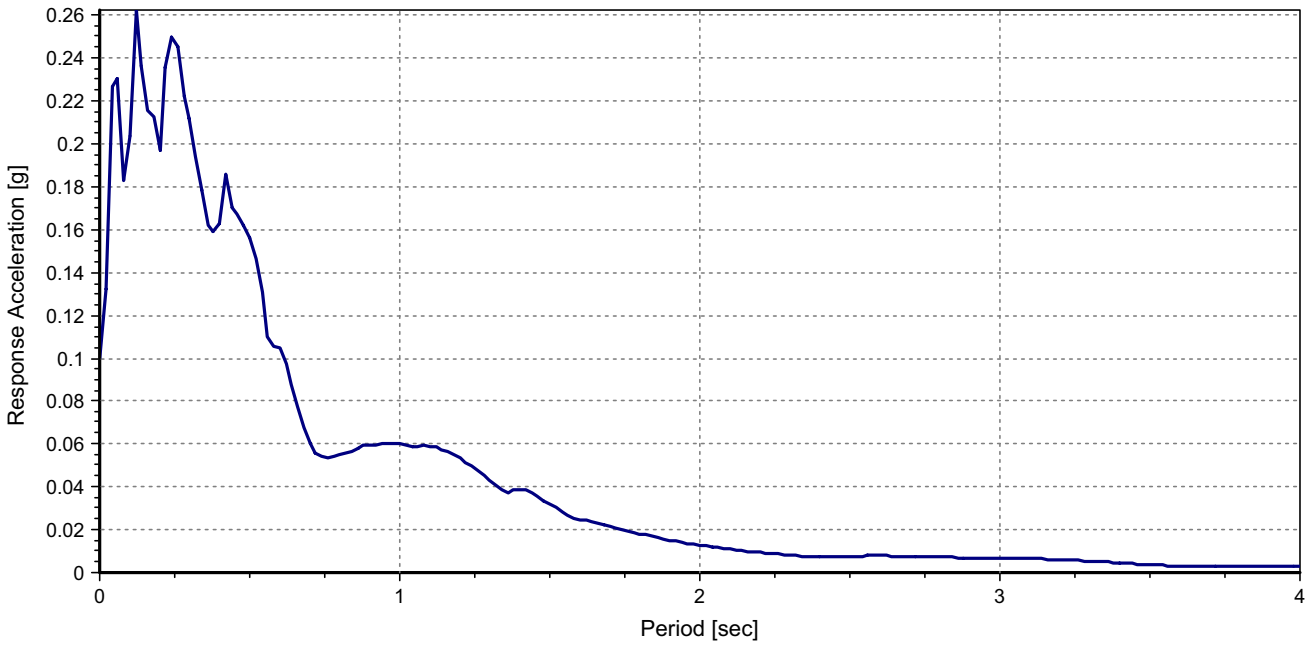

Fig. 19 Response spectra of horizontal El Centro earthquake wave (0.1 g)

Table 1 Physical and mechanical parameters of filling earth and foundation

	Foundation	Filling earth
Gravity (kN/m^3)	20.26	17
Water content (%)	3.6	–
Cohesion (kPa)	6.9	–
Internal frictional angle (°)	37.52	33

Fig. 20 Shaking table test model

The above comprehensive analysis shows that the frequency of seismic wave has a great influence on the seismic stability of rigid retaining wall and should be fully considered.

Conclusion

Some conclusions are obtained from the above analysis:

1. Aiming at the drawback existing in the analysis methods of seismic active earth pressure of rigid retaining wall, the time–frequency computational method of seismic active earth pressure of rigid retaining wall was proposed with the help of the horizontal slicing method and Hilbert–Huang transform. This method is a full 3D nonlinear time history analysis method, which not only can consider the effect of three factors (PGA, frequency and duration) of the seismic wave on the seismic earth pressure of rigid retaining wall, but also can provide some valuable references for the time–frequency seismic design of other retaining structures. At the same time, it is more accurate than the limit equilibrium method and coordinated deformation method.
2. The frequency of seismic wave has a significant effect on the resultant force of seismic active earth pressure and the critical rupture angle of backfill soil. The action position of resultant force is less affected by frequency, which should be considered in the calculation of active earth pressure for the rigid retaining wall. At the same time, according to the existing codes, the frequency of seismic wave is ignored in the seismic stability design

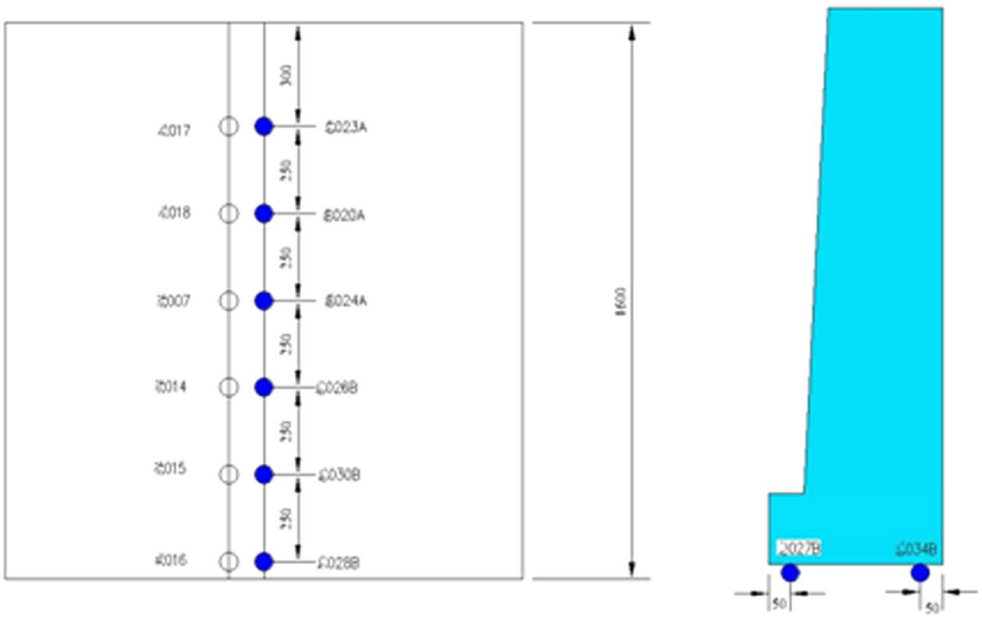

Fig. 21 Distribution of earth pressure monitoring points

Table 2 Comparison between the calculated results and the shaking table test results (Wolong–Wenchuan earthquake)

	Resultant force of active earth pressure (kN)				Acting point (h/H)			
	0.1 g	0.2 g	0.4 g	0.7 g	0.1 g	0.2 g	0.4 g	0.7 g
Shaking table test	5.48	5.65	6.75	8.97	0.34	0.38	0.39	0.34
Results of time–frequency analysis method	5.16	5.25	6.19	8.22	0.33	0.36	0.36	0.37
Results of limit equilibrium method	5.86	6.23	7.47	11.89	0.41	0.43	0.47	0.45
Results of coordinated deformation method	5.81	6.33	6.35	7.89	0.28	0.31	0.36	0.42
Error (%)—time–frequency analysis method	5.84	7.08	8.30	8.36	2.94	5.26	7.69	− 8.82
Error (%)—limit equilibrium method	− 6.93	− 10.27	− 10.67	− 32.55	− 20.59	− 13.16	− 20.51	− 32.35
Error (%)—coordinated deformation method	− 6.02	− 12.04	5.93	12.04	17.65	18.42	7.69	− 23.53

Table 3 Comparison between the calculated results and the shaking table test results (Kobe earthquake)

	Resultant force of active earth pressure (kN)				Acting point (h/H)			
	0.1 g	0.2 g	0.4 g	0.7 g	0.1 g	0.2 g	0.4 g	0.7 g
Shaking table test	6.02	7.09	7.87	12.98	0.33	0.34	0.37	0.35
Results of time–frequency analysis method	6.18	7.32	7.91	13.08	0.33	0.36	0.39	0.38
Results of limit equilibrium method	5.86	6.23	7.47	11.89	0.41	0.43	0.47	0.45
Results of coordinated deformation method	5.81	6.33	6.35	7.89	0.28	0.31	0.36	0.42
Error (%)—time–frequency analysis method	− 2.66	− 3.24	− 0.51	− 0.77	0.00	− 5.88	− 5.41	− 8.57
Error (%)—limit equilibrium method	2.66	12.13	5.08	8.40	− 24.24	− 26.47	− 27.03	− 28.57
Error (%)—coordinated deformation method	3.49	10.72	19.31	39.21	15.15	8.82	2.70	− 20.00

of rigid retaining wall, which may reduce the seismic safety reserve of retaining wall.

3. With the increase in seismic intensity, the active earth pressure gradually increases and the action position of resultant force moves up, while the critical rupture angle gradually decreases. Meanwhile, with the increase in frequency, the distribution of critical rupture angle and the active earth pressure force is "inverted saddle" and "saddle shaped," respectively. And they reach the maximum value when the frequency is close to the natural frequency of rigid retaining wall system. However, the action position of seismic active earth pressure is basically unchanged.

Table 4 Comparison between the calculated results and the shaking table test results (El Centro earthquake)

	Resultant force of active earth pressure (kN)				Acting point (h/H)			
	0.1 g	0.2 g	0.4 g	0.7 g	0.1 g	0.2 g	0.4 g	0.7 g
Shaking table test	5.63	5.89	7.13	10.02	0.33	0.36	0.4	0.37
Results of time–frequency analysis method	5.53	5.68	7.21	10.35	0.34	0.37	0.37	0.38
Results of limit equilibrium method	5.86	6.23	7.47	11.89	0.41	0.43	0.47	0.45
Results of coordinated deformation method	5.81	6.33	6.35	7.89	0.28	0.31	0.36	0.42
Error (%)—time–frequency analysis method	1.78	3.57	− 1.12	− 3.29	− 3.03	− 2.78	7.50	− 2.70
Error (%)—limit equilibrium method	− 4.09	− 5.77	− 4.77	− 18.66	− 24.24	− 19.44	− 17.50	− 21.62
Error (%)—coordinated deformation method	− 3.20	− 7.47	10.94	21.26	15.15	13.89	10.00	− 13.51

Error = (results from shaking table tests − results from calculated tests)/results from shaking table tests × 100%

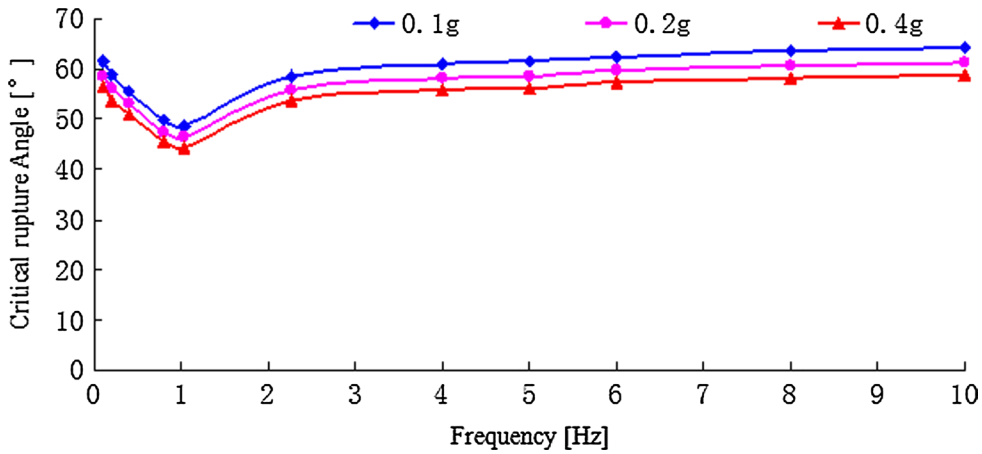

Fig. 22 Relationship between frequency and critical rupture angle

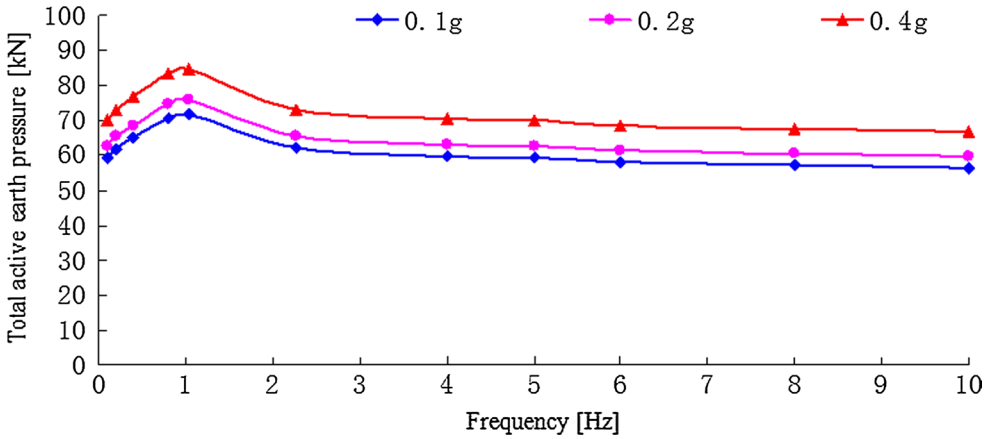

Fig. 23 Relationship between frequency and total active earth pressure

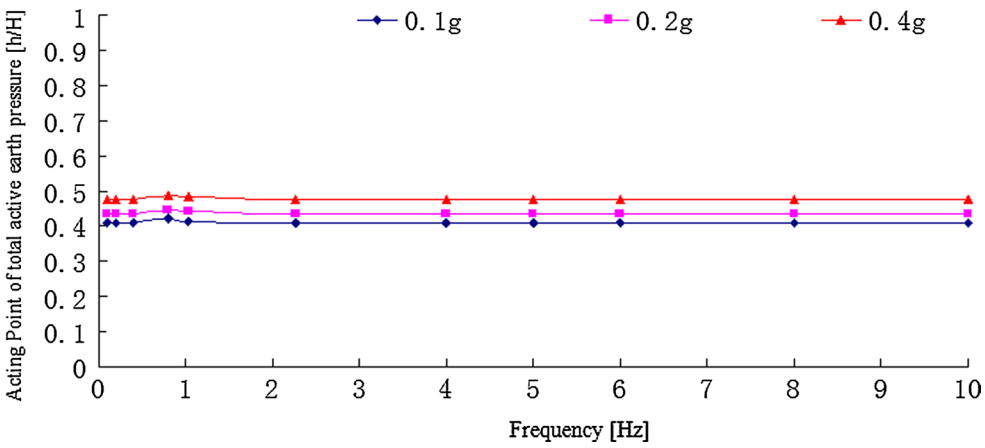

Fig. 24 Relationship between frequency and acting point of total active earth pressure

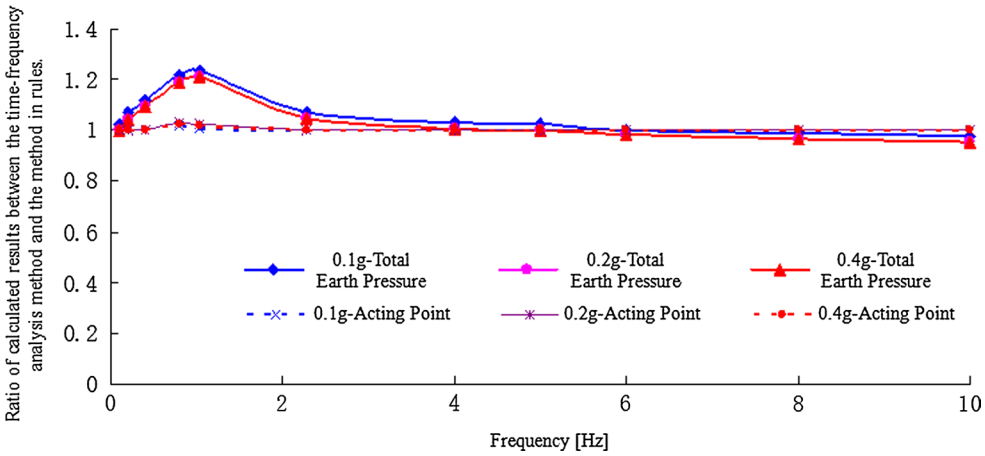

Fig. 25 Relationship between frequency and ratio of calculated results between time–frequency analysis method and the method in the rules

Acknowledgements This study is supported in part by Natural Science Foundation of China (Contract No. 51408510); Opening Fund of State Key Laboratory of Geohazard Prevention and Geoenvironment Protection (Chengdu University of Technology) (No. SKLGP2015K019); Sichuan Provincial Science and Technology Support Project (No. 2016GZ0338); the Fundamental Research Funds for the Central Universities (No. 2682016CX023); 2017–2019 Young Elite Scientisst Sponsorship Program by CAST; 2016–2018 Young Elite Scientisst Sponsorship Program by CAST/CSRME (YESS); Nanchang Railway Bureau Scientific Research Project (No. 20171106); and Education Department of Sichuan Province Scientific Research Project (No. 16ZB0012).

References

Ansal AM, Iyisan R, Güllü H (2001) Microtremor measurements for the microzonation of dinar. Pure Appl Geophys 158(12):2525–2541

Bird JF, Bommer JJ (2004) Earthquake losses due to ground failure. Eng Geol 75:147–179

Chigira M, Wu X, Inokuchi T, Wang G (2010) Landslides induced by the 2008 Wenchuan earthquake, Sichuan, China. Geomorphology 118:225–238

Choudhury D, Nimbalkar SS (2006) Pseudo-dynamic approach of seismic active earth pressure behind retaining wall. Geotech Geol Eng 24(5):1103–1113

Clough RW, Chopra AK (1966) Earthquake stress analysis in earth dams. J Eng Mech ASCE 92:197–211

Choudhury D, Singh S (2006) New approach for estimation of static and seismic active earth pressure. Geotech Geol Eng 24(1):117–127

Cui P, Zhu YY, Han YS, Chen XQ, Zhuang JQ (2009) The 12 May Wenchuan earthquake-induced landslide lakes: distribution and preliminary risk evaluation. Landslides 6:209–223

Cui K, Yang WH, Gou HY (2017) Experimental research and finite element analysis on the dynamic characteristics of concrete steel bridges with multi-cracks. J Vibroeng 19(6):4198–4209

Du XL (2009) Theories and methods of wave motion for engineering. Science Press, Beijing, pp 30–40

Gou HY, Shi XY, Zhou W, Cui K, Pu QH (2017) Dynamic performance of continuous railway bridges: Numerical analyses and field tests. Proc Inst Mech Eng F J Rail Rapid Transit. https://doi.org/10.1177/0954409717702019

Gou HY, Wang W, Shi XY, Pu QH, Kang R (2018) Behavior of steel-concrete composite cable anchorage system. Steel Compos Struct 26(1):115–123

Güllü H (2012) Prediction of peak ground acceleration by genetic expression programming and regression: a comparison using likelihood-based measure. Eng Geol 141–142:92–113

Güllü H (2013) On the prediction of shear wave velocity at local site of strong ground motion stations: an application using artificial intelligence. Bull Earthq Eng 11(4):969–997

Güllü H (2014a) A factorial experimental approach for effective dosage rate of stabilizer: an application for fine-grained soil treated with bottom ash. Soils Found 54(3):462–477
Güllü H (2014b) Function finding via genetic expression programming for strength and elastic properties of clay treated with bottom ash. Eng Appl Artif Intell 35:143–157
Güllü H (2015) Unconfined compressive strength and freeze–thaw resistance of fine-grained soil stabilised with bottom ash, lime and super-plasticiser. Road Mater Pavement Des 16(3):608–634
Güllü H, Erçelebi E (2007) A neural network approach for attenuation relationships: an application using strong ground motion data from Turkey. Eng Geol 93(3–4):65–81
Güllü H, Girisken S (2013) Performance of fine-grained soil treated with industrial wastewater sludge. Environ Earth Sci 70:777–788
Gullu H, Hazirbaba K (2010) Unconfined compressive strength and post-freeze–thaw behavior of fine-grained soils treated with geofiber and synthetic fluid. Cold Reg Sci Technol 62(2–3):142–150
Güllü H, Iyisan R (2016) A seismic hazard study through the comparison of ground motion prediction equations using the weighting factor of logic tree. J Earthq Eng 20(6):861–884
Güllü H, Khudir A (2015) Effect of freeze-thaw cycles on unconfined compressive strength of fine-grained soil treated with jute fiber, steel fiber and lime. Cold Reg Sci Technol 106–107:55–65
Güllü H, Pala M (2014) On the resonance effect by dynamic soil–structure interaction: a revelation study. Nat Hazards 72(2):827–847
Güllü H, Ansal AM, Özbay A (2008) Seismic hazard studies for Gaziantep city in South Anatolia of Turkey. Nat Hazards 44(1):19–50
Hazirbaba K, Gullu H (2010) California Bearing Ratio improvement and freeze-thaw performance of fine-grained soils treated with geofiber and synthetic fluid. Cold Reg Sci Technol 63(1–2):50–60
Huang NE, Shen Z, Long SR (1998) The empirical mode decomposition and Hilbert spectrum for nonlinear and non-stationary time series analysis. Proc R Soc 454(6):903–995
Hutchinson JN (1987) Mechanism producing large displacements in landslides on preexisting shears. Mem Soc Geol China 9:175–200
Jibson RW, Harp EL, Michael JA (2000) A method for producing digital probabilistic seismic landslide hazard maps. Eng Geol 58:271–289
Keefer DK (1984) Landslides caused by earthquakes. Geol Soc Am Bull 95:406–421
Khazai B, Sitar N (2003) Evaluation of factors controlling earthquake-induced landslides caused by Chi-Chi earthquake and comparison with the Northridge and Loma Prieta events. Eng Geol 71:79–95
Kumar J (2001) Seismic passive earth pressure coefficients for sands. Can Geotech J 38(4):876–881
Liao ZP (1996) Introduction to wave motion theories in engineering. Science Press, Beijing, pp 20–25
Lin YL, Yang GL, Zhao LH (2010) Horizontal slices analysis method for seismic earth pressure calculation. Chin J Rock Mech Eng 29(12):2581–2591
Lu TH (2002) A formula of active earth pressure including cohesion and adhesion. Rock Soil Mech 23(4):470–473
Ma HW, Wu B (2000) Elastic dynamics and its numerical method. China Building Industry Press, Beijing, pp 20–22
Madhav MR, Kameswara NS (1969) Earth pressure under seismic conditions. Soils Found 9(4):33–47
Magnitude 7.9 (2008) USGS, Eastern Sichuan, China. http://earthquake.usgs.gov/eqcenter/recenteqsww/Quakes/us2008ryan.php
Mononobe N (1924) Considerations on vertical earthquake motion relevant vibration problems. J Jpn Soc Civil Eng 10(5):1063–1094
Newmark NM (1965) Effects of earthquakes on dams and embankments. Geotechnical 15(2):59–139
Okabe N (1924) General theory on earth pressure and seismic stability of retaining wall and dam. J Jpn Soc Civ Eng 10(6):1277–1323
Prestininzi A, Romeo R (2000) Earthquake-induced ground failures in Italy. Eng Geol 58:387–397
Richards R, Elms DG (1979) Seismic behavior of gravity retaining walls. J Geotech Eng 105(4):444–449
Rodriguez CE, Bommer JJ, Chandler RJ (1999) Earthquake-induced landslides: 1980–1997. Soil Dyn Earthq Eng 18:325–346
Sassa K (1996) Prediction of earthquake induced landslides. In: Senneset K (ed) landslides. Balkema, Rotterdam, pp 115–132
Siddharthan RS, Norris G (1992) Simple rigid plastic model for seismic tilting of rigid walls. J Struct Eng 118(2):469–487
Smith HA, Wu WH (1997) Effective optimal structural control of soil–structure interaction systems. Earthq Eng Struct Dyn 26(5):549–570
Yang C, Feng N, Zhang J, Bi J, Zhang J (2015) Research on time-frequency analysis method of seismic stability of covering-layer type slope subjected to complex wave. Environ Earth Sci 74(6):5295–5306
Yang C, Jingyu Z, Lian J, Yu W, Zhang J (2016) Time-Frequency analysis method of acceleration amplification along hillslope. Environ Earth Sci 75(14):1095–1104
Yang CW, Zhang JJ, Wang ZZ, Hou JQ, Si CL (2018) Model test of failure modes of high embankment and aseismic measures for buried strike-slip fault movement. Environ Earth Sci. https://doi.org/10.1007/s12665-018-7324-7
Zeng X, Steedman RS (2000) Rotating block method for seismic displacement of gravity walls. J Geotech Geoenviron Eng 126(8):709–717
Zhang JJ, Feng J, Xiao SG, Liu CQ (2007) Discussions on two key technical problems for seismic design of retaining structures. J Southwest Jiaotong Univ 44(3):321–326